6A.1 INITIALIZING THE WRF MODEL WITH TROPICAL CYCLONE VITAL RECORD FOR TYPHOON FORECASTS BASED ON THE ENSEMBLE KALMAN FILTER ALGORITHM

Tien Duc Du[1], Thanh Ngo-Duc[2], and Chanh Kieu[3]*

[1]National Center for Hydro-Meteorological Forecasting, 4 Dang Thai Than Street, Hoan Kiem, Ha Noi, Vietnam

[2] Department of Space and Aeronautics, University of Science and Technology of Hanoi, Vietnam

[3]Department of Geological Sciences, Indiana University, Bloomington, IN 47405, USA

1. Introduction

Studies of tropical cyclone (TC) initialization for real-time forecasts have shown that incipient inner-core structure of TCs can have substantial impacts on TC initial adjustment and subsequent track and intensity development (see, e.g., Kurihara et al. 1993; Wang 1998; Hendricks et al. 2011, 2013; Nguyen and Chen 2011). Because of such sensitivity of TC development to the storm initial structure, enormous effort has been carried out to improve initial representation of TC inner-core structure in TC modeling applications. General approaches to improve the TC initial inner-core structure can be roughly divided into three categories including i) TC bogussing methods that replace an initially weak cyclonic perturbation by a bogus vortex with a prescribed intensity, ii) dynamical vortex initialization methods that use a numerical model to spin-up an initial vortex until the intensity of the model vortex matches with observed intensity, and iii) assimilation methods that directly ingest TC observations to enhance the TC representation in model initial condition.

Issues of complicated bogussing process and the related artificial numerical effects in the TC initialization have been effectively addressed with recent advances in data assimilation schemes (see, e.g., Zhang et al. 2011). Given demonstrated capability of a variant of the Ensemble Kalman filter algorithm, the so-called Local Ensemble Transform Kalman Fitter (LETKF), in context of TC forecasts (see, e.g., Miyoshi and Kunii 2012; Kieu et al. 2012, 2014; Cecelski et al. 2014), this study attempts to examine the effectiveness of the LETKF algorithm in assimilating the TCvital information into the WRF-ARW model for real-time TC forecasts in the north Western Pacific.basin Specifically, an innovative approach based on the real-time TCvital-synthetic observation that does not require the storm relocation or a bogus vortex will be presented. In addition to the real-time TCvital information, the atmospheric motion vector (AMV) data provided by the Cooperative Institute for Meteorological Satellite Studies (CIMSS) of the University of Wisconsin will be also assimilated to improve the large-scale environment that controls the TC steering flows, which could have significant effects on the TC track forecasts (Velden et. al. 1992; Kieu et al. 2012).

2. Experiment design

a. Model description and LETKF algorithm

In this study, the Weather Research and Forecasting model (WRF-ARW, version 3.2, Skamarock et al. 2008) was used with lateral boundary conditions updating every 6 hours from the National Centers for Environmental Prediction (NCEP) Global Forecasting System (GFS) real-time forecasts at resolution of 0.5^0 x 0.5^0. For the purpose of multiple-physics ensemble design, a set of physical parameterizations used in all ensemble experiments, more information see Kieu et al. (2012).

The LETKF algorithm (Hunt et al 2007) was used with a fixed multiplicative inflation factor of 1.1. To reduce spurious cross correlations in the LETKF algorithm, homogeneous covariance localization with a horizontal scale of 700 km is applied in all experiments such that far-field observations outside the TC main circulation will have minimum impacts on the TC inner region.

b. TCvital-based synthetic profile

This TCvital-based synthetic wind profile used in this study was based on a tangential wind profile proposed by Kieu and Zhang (2009), which is given by the following tangential wind structure:

$$V(r,\sigma) = V_m \frac{r}{r_m} \sin\left(\frac{\pi}{2}\sigma\right)^{1-\delta} \cos\left(\frac{\pi}{2}\sigma\right)^{\delta} \exp\{\frac{1}{b}[1-\left(\frac{r}{r_m}\right)^b]\} \quad (1)$$

where V_m is the VMAX, r_m is the RMW, r is the radius from the vortex center, b is a parameter that determines the horizontal shape of the wind profile, which is set equal to 0.7 by default, and

* Corresponding author: Chanh Kieu, Atmospheric Program, GY428A Geological Building, Department of Geological Sciences, Indiana University, Bloomington, IN 47405. Tel: 812-856-5704. Email: ckieu@indiana.edu.

$\delta \in [0, 1]$ is a free parameter determining the height of the VMAX relative to the surface (i.e., $\delta = 0$ corresponds to the maximum wind at the surface, whereas $\delta = 1$ corresponds to the maximum wind at the middle level, see Kieu et al. 2014b). With the tangential wind distribution as given by Eq. (1), the three-dimensional distribution of geopotential is then calculated by iteratively solving the nonlinear balance equation of the form (see Holton 2004).

$$\nabla^2 \Phi = \nabla \cdot (f \nabla \psi) - J\left(\frac{\partial \psi}{\partial x}, \frac{\partial \psi}{\partial y}\right) \quad (2)$$

In the final step, the balanced temperature profile is obtained by integrating the hydrostatic equation from the top down, based on the balanced geopotential distribution as obtained from Eq. (2).

c. Observation data and TC studied cases

Three TC cases in 2013 over the north Western Pacific basin are chosen (Super Typhoon Usagi on 18-19 September 2013, Typhoon Krosa from on 30-31 September 2013, and Super Typhoon Nari on 10-11 October 2013, see Figure 1). The Tropical Cyclone Vital Statistics Records provided by US Joint Typhoon Warning Center (JTWC) are used to provide all necessary inputs for constructing synthetic bogus structures and the AMV dataset from CIMSS-University of Wisconsin.

d. Ensemble experiments

Three sets of ensemble experiments are carried out to examine effects of the TCvital-based synthetic observation, the CIMSS-AMV data, as well as the effectiveness of the LETKF algorithm. The control experiment (CTRL) uses 21 members with different initials by adding noise to GFS/NCEP analysis. The second experiment DAMV also uses 21 members with different physical options, the same initial conditions from GFS/NCEP analysis and having CIMSS-AMV assimilation with LETKF. The last experiment DABV uses 21 members with different physical options, having the same initial conditions of CTRL and blending CIMSS-AMV and synthetic bogus vortex observation assimilation with LETKF. The same approach as in Zhang et al. (2006) for initialize cold-start background ensembles was used.

3. Results

a. Impact of the TCvital-based synthetic data

Figures 2 and 3 show that the TCvital-based synthetic increments (shaded) indeed capture a consistently deep wind structure at all levels with strong cyclonic wind components coming from two main reasons. First, the storm intensity in the GFS background is generally much weaker than the observed intensity when TCs are sufficiently strong (cf. Figure 1). Secondly, the large synthetic increments are due to the fact that the GFS storm centers are not the same as those reported in TCvitals. Given the above distribution of the synthetic wind increments with a dipole structure for both the zonal and meridional winds around the vortex center as seen in Figs. 2 -4, it is of importance to notice that the LETKF analysis increments could exhibit similar patterns and magnitudes at all levels. Specifically, consistent enhancement of the TC inner-core circulation with two peaks of analysis wind increments > 15 m s^{-1} (negative to the north and positive to the south of the vortex center) is observed in all three cases, which indicate the influence of the synthetic increments in correcting both the storm intensity and the storm initial location. Of further interest is that the analysis increments could capture strong asymmetry of the zonal wind due to existence of strong easterly mean flows in the WPAC basin (cf. Figs 2a, d, g). In this regard, the TCvital-based synthetic profile data appears to not only enhance the TC intensity but also help re-locate the GFS initial storm center as expected.

The centers of the wind dipoles in all analysis increments do not completely coincide with the synthetic increments at higher levels (see, e.g., Fig. 2h or 3h). This is due to the fact that real storms are often tilted with height that the TCvital-based synthetic profiles given by Eq. (1) cannot capture. Such influence of vortex tilting on assimilating a storm vertical structure and the extent to which the TCvital-based synthetic information can be assimilated in the GFS analysis is seen most clearly in the vertical cross sections through the storm center (Figure 5). In addition to the vortex tilting issue, the storm size could play some role in assimilating the synthetic information. Figs 3 and 5 show the consistent of analysis increments and synthetic increments for the cases of STYs Usagi and Krosa, whereas the case of STY Nari tends to have a larger discrepancy between the synthetic and the analysis increments due to Nari's smaller inner-core size (~ $3^0 \times 3^0$ instead of $5^0 \times 5^0$ as for the cases of Usagi and Krosa). Another significant benefit of assimilation of TCvital-based synthetic profiles is that TCvitals could allow for spread of the surface information to higher levels (cf. Figure 4), which is expected if the TCs are sufficiently strong that they possess a coherent structure thorough the troposphere as implied from the surface observed information.

b. Impact of the AMV data

In Figure 5, consistent with characteristics of the AMV data, much higher density of the AMV data points is found at upper levels above 300 hPa, whereas data points at lower levels are mainly in the peripheral area of the storm central region. As such, assimilation of the AMV data does not seem to capture much information about either the storm inner-core structure or the storm intensity at lower levels. As displayed in Figure 5, the analysis wind vector increments show a general enhancement with a broader cyclonic circulation at 200 hPa similar to the observed vector increments. Such cyclonic increments at upper levels indeed confirm that the anticyclonic circulation associated with TC outflows in the GFS analysis is overall weaker than the satellite observation, which corresponds to a weaker intensity at the surface.

With capability of enhancing the storm-scale structure by the TCvital-based synthetic information and the large-scale environmental flows by the AMV data, it is thus natural to consider next a combination of these data sources to improve both the storm-scale structure and the environmental flow. Similar to Figure 5, Figure 6 shows comparison of the observed and the analysis increments for wind vectors in the DABV experiments for three different storms. As expected, the cyclonic vector wind increments associated with the TCvital-based synthetic information show consistent enhancement in the storm central region at the lower levels, whereas the upper level circulation flow correctly captures the stronger outflow as dictated by the AMV data similar to Figure 5. The consistency in the LETKF analysis increments and the synthetic/AMV increments demonstrates that our proposed approach of blending the TCvital-based synthetic profiles and the AMV data is capable of improving representation of TC circulations both in the inner-core region and the large-scale environment with the LETKF algorithm.

Despite some competition of the TCvital and the AMV data in the storm lower inner-core region due to the slight overlap, we should emphasize again that the TCvital synthetic data is mostly from surface up to 300 hPa and confined within the storm area, whereas the AMV data is distributed mainly outside the storm area and above 300 hPa. In this sense, the two sets of dataset are complementary rather than directly competing with each other and the negative influence of the interference of these data sources is thus minimal. Of course, there are some disadvantages of the synthetic data in effectively correcting storm initial locations, or uncertainties in the storm vertical structures that the TCvital-based synthetic profiles may not fully capture. However, the best evaluation of the effectiveness of our blending approach could be justified from examination of the track and intensity forecasts errors along with the ensemble spread that we now turn into.

c. Track and intensity forecast performance

With improvement in the large-scale environment in the DAMV experiments and use of the multiple-physics LETKF algorithm to correct model errors, it is of interest to note that the northward bias of the track bias in the CTRL forecast is generally reduced in all DAMV experiments (cf. Figs. 7b, c, h). The much larger ensemble spread in the DAMV experiments is attributed to several factors including i) better sampling of the initial condition uncertainties by the LETKF algorithm, ii) use of multiple-physics option that could take into account the model errors, iii) use of different boundary conditions in our WRF-LETKF design, and iv) different large-scale environment for different ensemble members after assimilating the AMV data. These examples show the role of the LETKF algorithm in improving the track forecasts that the simple randomly perturbed initial conditions in the CTRL experiments which could not accomplish.

While the initial vortex inner-core structure is further improved with the use of TCvital-based synthetic observation in the DABV experiments, there is no additional improvement both in terms of track bias as well as the ensemble track spread in the DABV track forecasts (Figs 7c, f, i). Physically, such negligible effect of the vortex strength and inner-core structures to the track forecast for the strong intensity cycles is not uncommon, because the overall movement of the storm track tends to be determined more by the large-scale environment rather than the storm initial structure, especially at longer lead times. While a vortex initial structure could have significant influence to the storm development, especially during the early development, weak dependence of TC track on storm initial strength is statistically consistent with various real-time TC forecasts using different operational models as reported, e.g., in Tallapragada et al. (2015).

In terms of intensity forecasts, in Figure 8, the first distinct difference intensity forecasts among the CTRL, the DAMV, and the DABV experiments is ensemble spread. While the CTRL ensemble show a small spread as in the track forecasts, one notices a much larger intensity spread in both the DAMV and the DABV forecasts as compared to the CTRL. For either the DAMV or the DABV forecasts, the spread is small during the first 12 hours, but it quickly grows and covers a wide range of intensity variations after just 18 hours into integration. The larger spread in DAMV intensity forecasts demonstrates the roles of the multiple-physics LETKF design in capturing uncertainties in TC development that the CTRL could not obtain with simple randomly perturbed initial conditions. Secondly, the TCvital-based synthetic profiles are able to correct the storm initial intensity after being assimilated, thus explaining for better fit of the DABV storm initial intensity with the observed intensity, which is not seen in the DAMV experiments. As seen in Figs. 8c, f, i, the VMAX in all DABV forecasts has closer values to the observed intensity right at the initial time$t = 0$, suggesting the complementary roles of the AMV and the TCvital-based synthetic data in enhancing the storm intensity.

In Figure 9, the DAMV shows the best track forecast performance with noticeable improvement from 1-day to 3-day lead times at 95% statistical significance, which is consistent with generally improved large-scale environmental condition after assimilating the AMV data. Likewise, the DABV has slight track improvement relative to CTRL with most reduction in the track forecast errors between 48 and 84 hours. This demonstrates the role of the AMV data in correcting the large-scale environmental condition, which is lacked in the CTRL forecasts. Although the track forecast errors at the 4-day and 5-day lead times are not of statistical significance, it is interesting to note however that the DABV track forecast skill is somehow deteriorated specifically at the 5-day lead time as compared to the CTRL forecasts, despite similar use of the AMV data as in the DAMV experiments.

Unlike the track errors, intensity errors show significant benefit with assimilation of TCvital synthetic profiles at longer ranges. While the DABV has similar absolute and bias errors as the CTRL errors from 0-3 days, it possesses the lowest errors overall at 4-5 day lead times with the absolute errors ~ 13 m s^{-1} at the 5-day lead time (Figure 9b). In contrast, the CTRL intensity errors show a dominant tendency of underestimation of the storm intensity at the 4-5 day lead times (Figure 9c). The DAMV experiments show similar improvement in intensity forecasts at the 4-5 day lead times as compared to the CTRL experiments. This suggests that improvement in the large-scale environment plays a key role in the intensity improvement at long ranges, even though it would take several days to be realized, thus confirming the importance of the large-scale environmental flows in helping storm to develop consistently. The use of TCvital-based synthetic profiles to enhance vortex inner-structure appears to further aid model storms to more quickly adapt to the ambient environment, which can be seen in Figure 8 as a faster spin-up of the model storm during the first 18 hours into integration as compared to the DAMV experiments. This may explain slightly larger intensity errors in the DABV experiments during 0-72 hours, but eventually the DABV could capture better the storm development and thus possess good performance at the 4-5 day lead times.

Along with positive impacts on improvement of the track and intensity forecast performance at long ranges from both the AMV and TCvital synthetic data, it should be mentioned that use of the multiple physics in the LETKF system to represent model errors is another significant factor in increasing the ensemble spread and capturing larger uncertainties (Figure 10).

4. Conclusions

In this study, a method to directly assimilate tropical cyclone vital records (TCvitals) into the WRF model has been presented for real-time tropical cyclone (TC) forecast applications, based on the local transform ensemble Kalman filter (LETKF) algorithm. The proposed method consists of three basic steps: 1) generate a dynamically consistent three-dimensional synthetic profile for the vortex structure based on the TCvital information to enhance axisymmetric components of the TC inner-core circulation, and 2) blend the synthetic profile with the CIMSS-AMV data to further augment representation of the large-scale steering flows, and 3) assimilate the blended data into GFS analyses using the LETKF algorithm.

Preliminary experiments of the blending data approach with the WRF-LETKF system for several selected TCs in the north Western Pacific basin showed that our proposed approach could effectively enhance both the storm inner-core circulation and the ambient environment that these typhoons are embedded in as compared to control experiments. Specifically, TCvital-based synthetic profiles could add more inner-core structure to the GFS initial vortices thorough the troposphere, and help reducing model initial spin-up of the GFS vortices. Although the added inner-core structure does not seem to help reduce intensity errors at 0-3 days, it could shows improvement in the longer range intensity forecast skill. Likewise, the AMV data corrects the environmental steering flows, and has significant influence on TC development at longer lead times as well. Combination of the TCvital and the AMV data along with use of multiple-physics options in our WRF-LETKF system to represent model errors showed that both the track and intensity forecast errors can be reduced, albeit the error reduction is not of statistical significance due to a limited sample size. It was noticed, however, that track forecast errors after assimilating the blended TCvital profile and the AMV data appear to be larger than the control experiments at the 5-day lead time. While we have not fully understood such behaviors, the overall reduction in both the intensity bias and the spin-up time of the model vortex suggests that use of the TCvital-based synthetic information could allow for model storms to quicker adjust to the ambient environment.

The proposed approach will be most beneficial for future TC models that are initialized directly from very high resolution global models for which storm initial location is sufficiently accurate (within a given storm location uncertainty) that there is no need to carry out artificial vortex removal or insertion.

Acknowledgement

This research was partially supported by the start-up funding provided by Indiana University.

References

Cecelski, S., D.-L. Zhang, and T. Miyoshi, 2014: Genesis of Hurricane Julia (2010) within an African Easterly wave: Developing and non-developing members from WRF-LETKF ensemble forecasts. *J.Atmos. Sci.*, **71**, 2763-2781.

Holton, J. R., 2004: *Introduction to Dynamic Meteorology,* Elsevier Academic Press.

Hunt, B. R., E. J. Kostelich, and I. Szunyogh, 2007: Efficient data assimilation for spatiotemporal chaos: A local ensemble transform Kalman Filter. *Physica D*, **230**, 112–126.

Kieu, C. Q., and D.-L. Zhang, 2009: An analytical model for the rapid intensification of tropical cyclones. *Quart. J. Roy. Meteor. Soc.*, **135**, 1336-1349.

Kieu, C. Q., M. T. Nguyen, T. M. Hoang, T. Ngo-Duc, 2012: Sensitivity of the Track and Intensity Forecasts of Typhoon Megi (2010) to Satellite-Derived Atmospheric Motion Vectors with the Ensemble Kalman Filter. *J. Atmos. Oceanic Technol.*, **29**, 1794–1810.

Kieu, C. Q., V., Tallapragada, and W. Hogsett, 2014b: On the onset of the tropical cyclone rapid intensification in the HWRF model. *Geophys. Res. Lett*., **9**, 3298-3306.

Miyoshi, T. and M. Kunii, 2012: The Local Ensemble Transform Kalman Filter with the Weather Research and Forecasting Model: Experiments with Real Observations. *Pure and Appl. Geophys.*, **169**, 321-333.

Skamarock, W. C., J. B. Klemp, J. Dudhia, D. O. Gill, D. M. Barker, M. G. Duda, X. Y. Huang, W. Wang, and J. G. Powers, 2008: A description of the Advanced Research WRF Version 3. NCAR Tech. Note NCAR/TN-475+STR, 113 pp.

Tallapragada, V., C. Q. Kieu, Y. Kwon, Q. Liu, S. Trahan, Z. Zhang, M. Tong, B. Strahl, 2015: Real-Time Forecasts for the 2012 North-Western Pacific Typhoon Season using the NCEP Operational HWRF. Wea. and Forecasting, 30, 1355-1373.

Velden, C. S., C. M. Hayden, W. P. Menzel, J. L. Franklin, and J. S. Lynch, 1992: The impact of satellite-derived winds on numerical hurricane track forecasting. *Wea. Forecasting,* **7**, 107–118.

Zhang, F., Y. Weng, J. F. Gamache, and F. D. Marks, 2011: Performance of convection-permitting hurricane initialization and prediction during 2008–2010 with ensemble data assimilation of inner-core airborne Doppler radar observations. *Geophys. Res. Lett.*, **38**, 15, doi:10.1029/2011GL048469.

Zou, X. and Q. Xiao, 2000: Studies on the Initialization and Simulation of a Mature Hurricane Using a Variational Bogus Data Assimilation Scheme. J. Atmos. Sci., 57, 836–860.

Figures

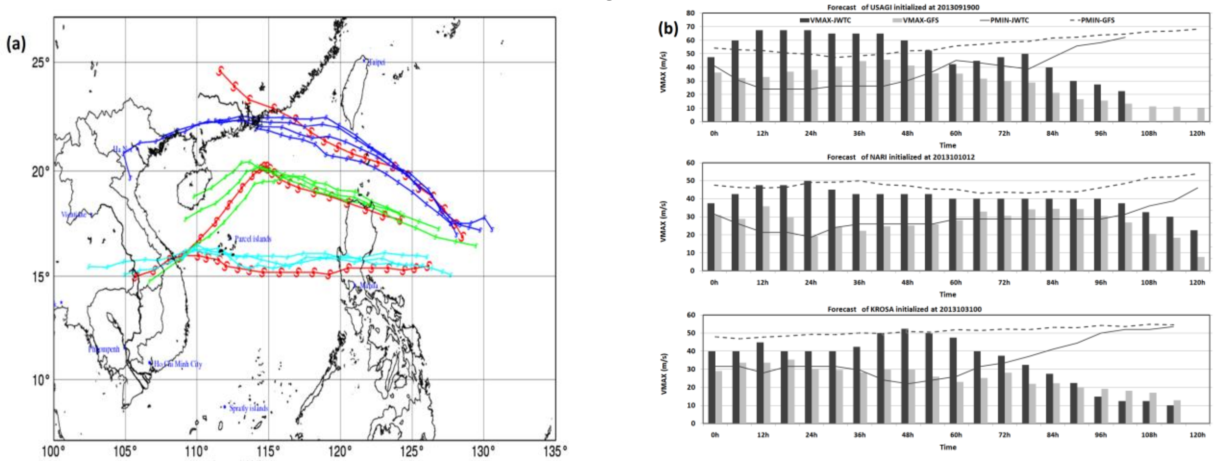

Figure 1. (a) GFS/NCEP 5-day track forecasts and the corresponding best tracks (red) for three selected TC cases including Super Typhoon Usagi (blue) valid at 0000 UTC Sep 18, 1200 UTC Sep 18, and 0000 UTC Sep 19, 2013, Super Typhoon Nari (cyan) at 0000 UTC, Oct 10, 12000 UTC Oct 10, and 0000 UTC Oct 11, 2013, and Typhoon Krosa (green) at 0000 UTC Oct 30, 12000 UTC Oct 30, and 0000 UTC Oct 31, 2013; (b) Corresponding GFS 5-day intensity forecasts and the observed intensity for Usagi at 0000 UTC Sep 19 2013, Nari at 12000 UTC Oct 10 2013, and Krosa at 0000 UTC Oct 31, 2013. Columns denote the VMAX (unit ms^{-1}) from the GFS forecasts (gray) and from the best track (black). Solid lines denotes the observed PMIN (unit hPa), and dash lines are for the GFS forecasts of the PMIN.

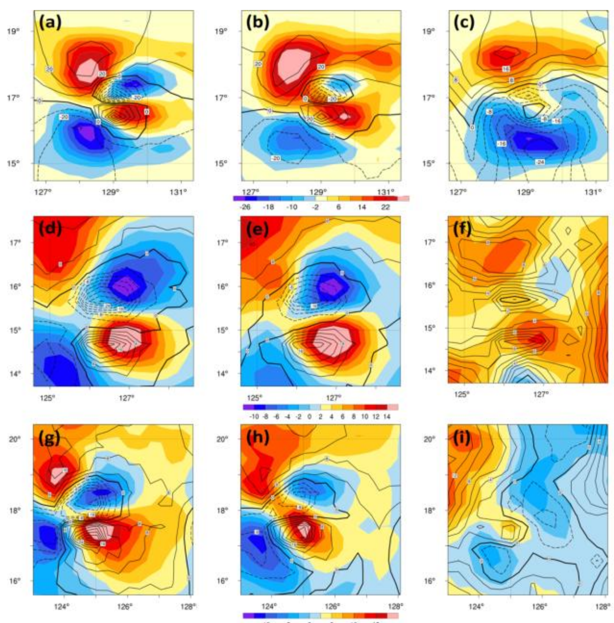

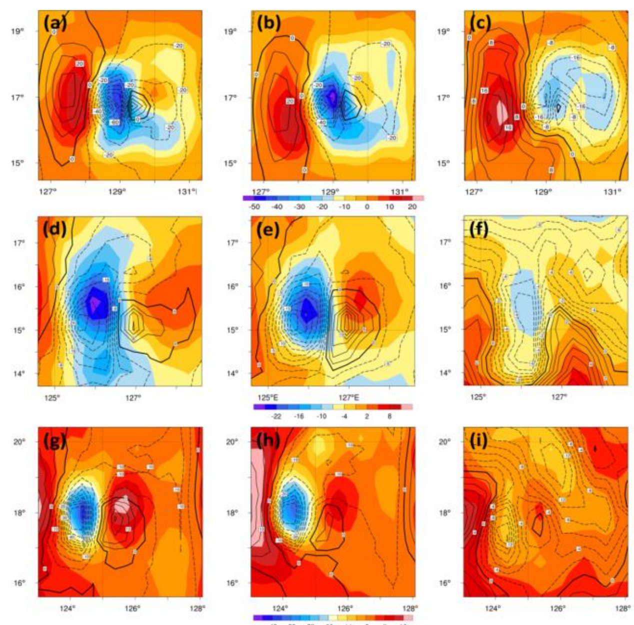

Figure 2. Horizontal cross sections at three different levels $p = $ 850mb (left panels), 500mb (middle panels) and 200mb (right panels) of the zonal u-wind increments (unit ms^{-1}), which are obtained from the TCvital-based synthetic profiles (contours) and the analysis increments obtained from the WRF-LETKF system (shaded) for three selected cycles of (a)-(c) Typhoon Usagi valid at 0000 UTC 20 Sep 2013, (d)-(f), Typhoon Nari valid at 0000 UTC 10 Oct 2013, and (g)-(i) Typhoon Krosa valid at 0000 UTC 31 Oct 2013. Solid contours are for the

Figure 3. Similar to Figure 2 but for meridional v-wind increments

positive values, and dashed contours are for negative values. The bold solid lines are zero contours.

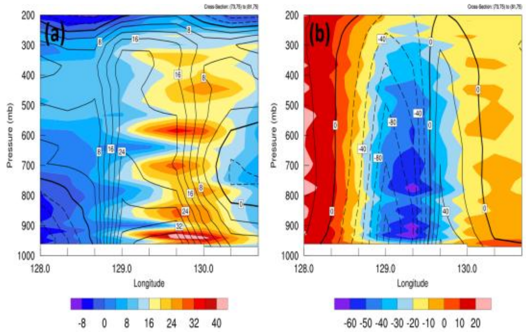

Figure 4. West-East vertical cross sections of the observed zonal u-wind increments (left panels) and v-wind component (right panels) obtained from the TCvital-based synthetic observation (contour) and the corresponding analysis increments (shaded) obtained from the WRF-LETKF system for the case of Typhoon Usagi valid at 0000 UTC 20 Sep 2013 (a, b)

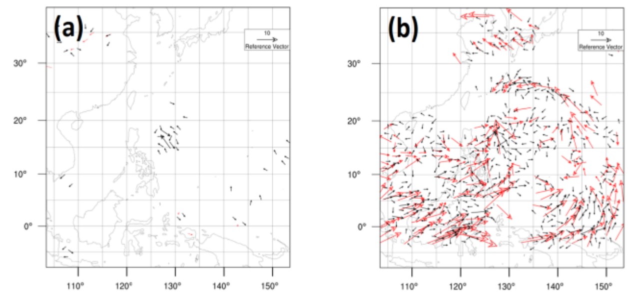

Figure 5. Horizontal distributions of the CIMSS-AMV wind vector increments (black) and the analysis wind vector increments obtained from the WRF-LETKF system (red) at two levels $p = 500$mb (left panels) and 200mb (right panels) for the entire outermost domain (36 km) for the case of Usagi valid at 0000 UTC 20 Sep 2013 (a, b)

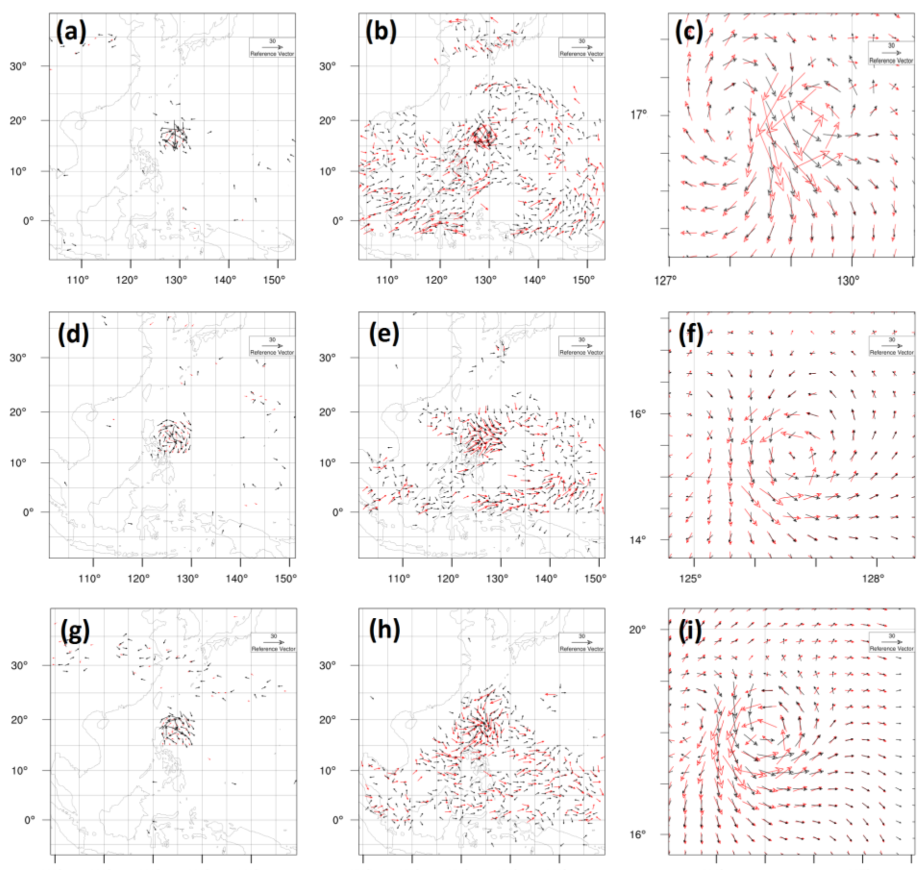

Figure 6. Horizontal distributions of the observed wind vector increments (black vectors) obtained from the DABV experiments with blending of the TCvital profiles and the AMV data, and analysis wind vector increments obtained from the WRF-LETKF system (red vectors) at levels $p = 500$mb (left panels), 200mb (middle panels), and zooming in within the TC region (right panels) at level 990mb for (a)-(c) Typhoon Usagi valid at 0000 UTC 20 Sep 2013; (d)-(e)

Typhoon Nari valid at 0000 UTC 10 Oct 2013. Only vector increments with amplitude larger than 1 m s^{-1} are displayed.

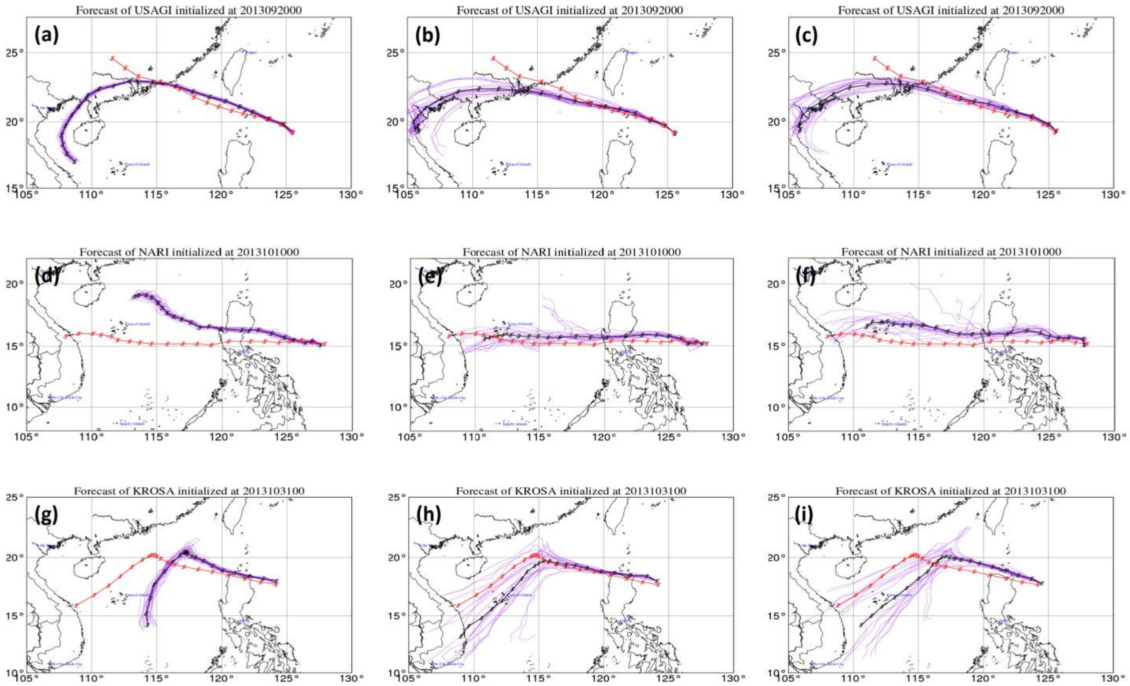

Figure 7. Ensemble track forecasts for the CTRL experiments (left panels), the DAMV experiments (middle panels), and the DABV experiment (right panels) for (a)-(c) Typhoon Usagi valid at 0000 UTC 20 Sep 2013, (d)-(f) Typhoon Nari valid at 1000 UTC 10 Oct 2013, and (g)-(i) Typhoon Krosa valid at 0000 UTC 31 Oct 2013. Purple lines denote ensemble member forecasts, black lines denote the ensemble mean, and red lines denote best tracks.

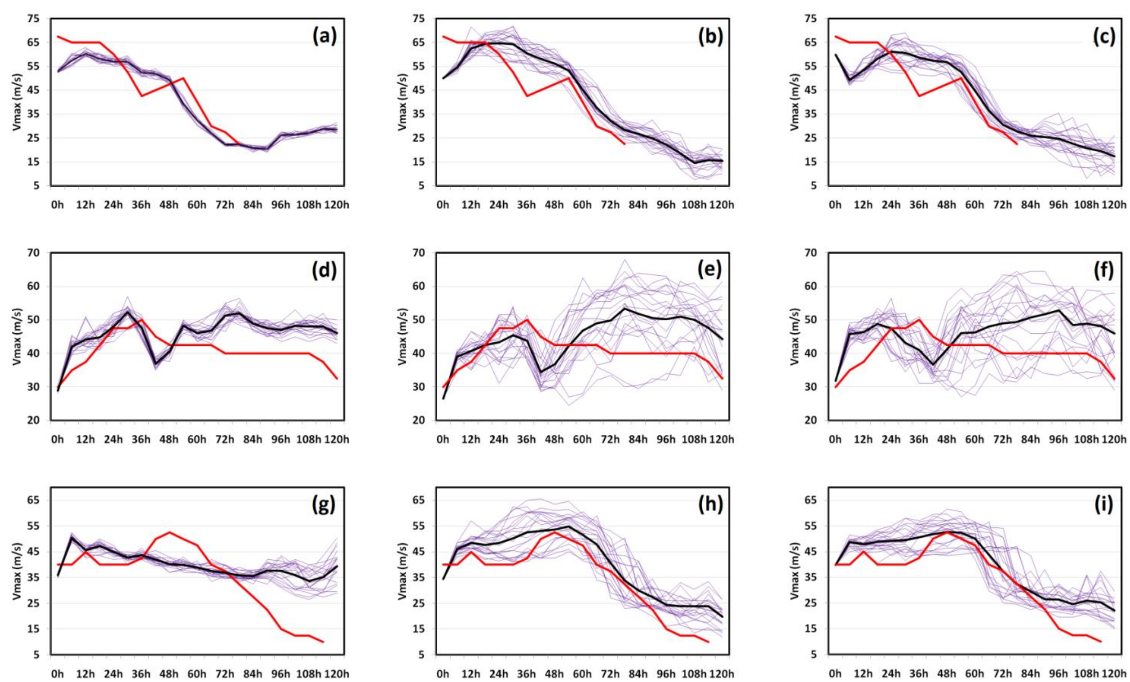

Figure 8. Similar to figure 7 but for the time series of the maximum 10-m wind (VMAX).

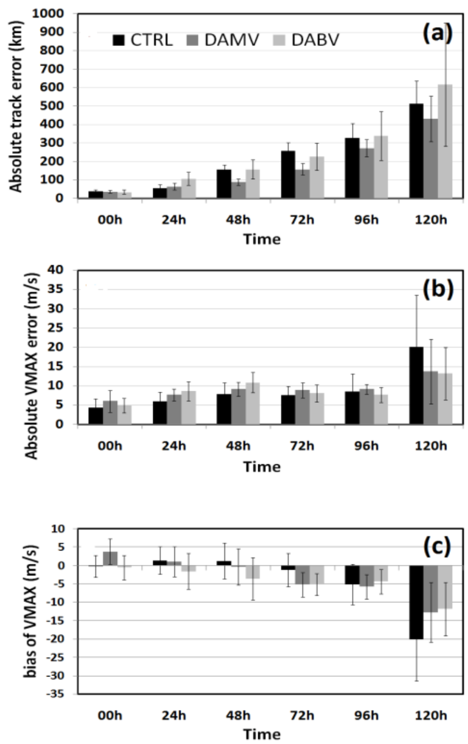

Figure 9. Verification of (a) the absolute track forecast errors (columns, unit km) for the CTRL (black), the DAMV (gray), and the DABV (light gray) experiments; (b)-(c) similar to (a) but for the mean absolute VMAX error (unit, m s^{-1}) and the mean VMAX bias (unit m s^{-1}). Error bars denote the 95% confidence intervals

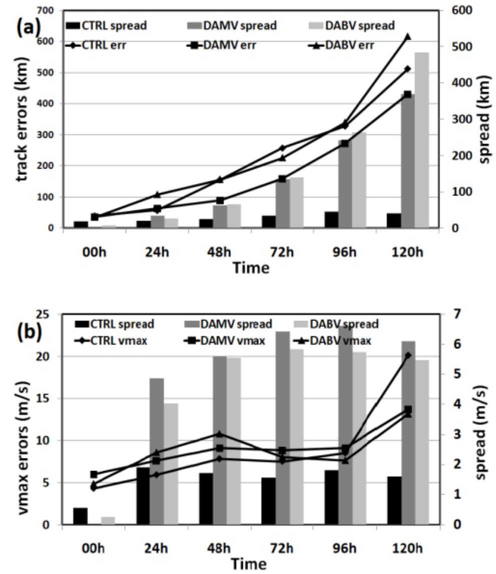

Figure 10. (a) Time series of the ensemble track spread (bars, unit km) and the track errors (solid lines, unit km); (b) similar to (a) but for the absolute intensity spread and error obtained from the CTRL experiments (black bars and diamond line), the DAMV experiments (gray bars and square line), and the DABV experiments (light gray bars and triangle line)